Systemic 5-fluorouracil drives competitive release of multidrug-resistant, virulent *Enterococcus faecalis* lineages in the gut

Jinzhou Ye[1]†, Beibei Chen[1,2]†, Yazhou Xu[3]†, Danzhi Wu[1]†, Qiulong Tan[4], Wenjun Chen[3], Xing Li[5]*, Chao Wang[6]*, Xinhai Chen[1,7,8]*

[1]Insititute of Infectious Diseases, Shenzhen Bay Laboratory, Shenzhen 518132, China.

[2]School of Biology and Biological Engineering, South China University of Technology, Guangzhou 510006, China.

[3]Department of Laboratory Medicine, Third Affiliated Hospital of Sun Yat-Sen University, Tianhe Road 600#, Guangzhou 510630, China.

[4]Rare Disease Center, Shenzhen Medical Academy of Research and Translation, Shenzhen 518107, China.

[5]Medical Examination Center and Department of Medical Oncology, the Third Affiliated Hospital of Sun Yat-sen University, Tianhe Road 600#, Guangzhou, 510630, China.

[6]Institute of Systems and Physical Biology, Shenzhen Bay Laboratory, Shenzhen 518132, China

[7]Shenzhen Medical Academy of Research and Translation, Shenzhen 518107, China.

[8]Guangdong Provincial Key Laboratory of Infection Immunity and Inflammation, Shenzhen 518060, China

*Corresponding author. Email: xinhaichen@szbl.ac.cn (X.C.); chaowang@szbl.ac.cn (C.W.); lixing9@mail.sysu.edu.cn (X.L.)

†These authors contributed equally to this work.

Abstract

Systemic chemotherapy perturbs the intestinal ecosystem, yet its impact on within-species population dynamics remains poorly understood. Here, we show that systemic 5-fluorouracil (5FU) exerts strong strain-selective pressure on gut *Enterococcus faecalis*, reshaping population structure without altering overall abundance. In patients receiving 5FU and in murine models, intestinal exposure to the drug suppresses 5FU-sensitive lineages while enriching pre-existing resistant clones. Resistant lineages exhibit enhanced 5FU detoxification associated with PreT/A-like enzymes and a redox-buffering program that preserves NADPH through disruption of CDP-ribitol-dependent metabolism. Drug-sensitive strains suppress resistant competitors via secreted inhibitory activity; 5FU eliminates this constraint, enabling competitive release and clonal expansion of resistant lineages. These 5FU-selected lineages display multidrug resistance, including elevated cephalosporin tolerance linked to upregulated penicillin-binding proteins, and exhibit increased virulence *in vivo*. Thus, systemic chemotherapy can inadvertently select high-risk pathobiont lineages through strain-level competitive release, generating intestinal reservoirs of multidrug-resistant and virulent bacteria. These findings highlight the importance of strain-resolved microbiome analysis and reveal an ecological mechanism by which anticancer therapy may increase infectious risk.

Introduction

Chemotherapy imposes systemic perturbations that extend beyond direct tumor cytotoxicity, prominently affecting mucosal tissues and the intestinal ecosystem. Mucosal barrier injury is common across anti-cancer regimens and has been increasingly linked directly or indirectly to shifts in the oral and gut microbiota, with implications for inflammation, permeability, and infectious complications[1,2]. In parallel, the gut microbiota can modulate chemotherapy outcomes through xenobiotic metabolism, enzymatically transforming drugs and thereby altering efficacy or toxicity[3-5]. Despite rapid progress, much of the clinical literature still summarizes chemotherapy-microbiome interactions at coarse taxonomic resolution, potentially obscuring within-species dynamics that can be biologically and clinically consequential[6-8].

Fluoropyrimidines provide a powerful model for dissecting such interactions. 5-fluorouracil (5FU) is cleared in humans to the inactive metabolite dihydrofluorouracil (DHFU) by host dihydropyrimidine dehydrogenase (DPYD)[9], and recent work has revealed that gut bacteria can catalyze an analogous inactivation via the bacterial *preTA* operon, with measurable phenotypic consequences *in vivo*[10,11]. These observations raise the question of whether systemic chemotherapy can act as an ecological pressure in the gut that selectively remodels within-species population structure rather than simply shifting species abundance. This question is particularly urgent for *Enterococcus faecalis*, a prevalent gut colonizer that can become a major opportunistic pathogen in immunocompromised hosts and is notable for genomic plasticity and antibiotic resistance[1]. Enterococci also participate in intense inter-strain competition, including bacteriocin/enterocin-mediated antagonism that can shape niche occupancy in complex gut communities[12]. Because strain variation can be as important as species variation for microbial function and epidemiology, species-level profiling alone may fail to capture

shifts in colonization risk or the emergence of high-risk lineages[6].

Here, we investigated whether systemic chemotherapy can act as an ecological force that reshapes within-species population structure in the gut. Focusing on *E. faecalis*, we show that systemic 5FU imposes strong strain-selective pressure in the intestinal environment without altering overall species abundance. Instead, 5FU promotes the expansion of pre-existing drug-resistant lineages by relieving competitive constraints within the gut. These findings reveal a mechanism by which systemic chemotherapy can drive strain-level population restructuring of a gut pathobiont and highlight the importance of resolving microbiome dynamics beyond species-level abundance in the context of cancer therapy.

Results

5FU therapy enriches intestinal *E. faecalis* subpopulation with reduced 5FU susceptibility

To investigate how anticancer agents reshape gut-associated bacterial populations, particularly under conditions of ecological perturbation, we curated a panel of 217 FDA-approved anticancer drugs (Table. S1). Given that chemotherapy can disrupt microbial community structure and enable the expansion of both resident commensals and opportunistic pathogens, we systematically evaluated their antibacterial activity at three concentrations (2, 20, and 200 μM) using *Escherichia coli* and *Staphylococcus aureus* as representative Gram-negative and Gram-positive organisms, respectively. Across this panel, 22.6% of the tested compounds exhibited detectable growth-inhibitory activity at 200 μM (Fig. S1A; Table. S1). Notably, a greater number of compounds were active against *S. aureus*, and effective concentrations were generally lower compared with those required to inhibit *E. coli* (Table S1). Among the anticancer agents displaying antibacterial activity, 5-fluorouracil

(5FU) demonstrated the most potent and broad-spectrum inhibitory effects (Fig. 1, A and B). Minimum inhibitory concentration (MIC) testing further revealed that 5FU exhibited MIC values below 1 μg/mL for most Gram-positive bacteria tested, although the MIC against *Listeria monocytogenes* was modestly higher (3 μg/mL) (Fig. 1C). In contrast, among Gram-negative organisms, 5FU showed the lowest MIC against *E. coli* (50 μg/mL), whereas MIC values exceeded 400 μg/mL for other clinically relevant pathogens, including *Klebsiella pneumoniae*, *Salmonella typhimurium*, *Pseudomonas aeruginosa*, and *Acinetobacter baumannii* (Fig. 1C). Growth curve analysis confirmed these MIC findings, demonstrating substantially greater growth inhibition in Gram-positive bacteria (Fig. 1D; Fig. S1B). Notably, among Gram-positive species, *Enterococcus faecalis* exhibited the highest sensitivity to 5FU, with an MIC of 0.19 μg/mL (Fig. 1C). Moreover, in liquid culture, 5FU at concentrations as low as 0.098 μg/mL was sufficient to markedly suppress *E. faecalis* growth (Fig. 1D). This inhibitory effect was further validated across multiple clinical *E. faecalis* isolates from infected patients (Fig. S1C).

Given the high sensitivity of *E. faecalis* to 5FU and its primarily intravenous administration, we asked whether intestinal drug concentrations in patients receiving 5FU therapy are sufficient to inhibit this organism. Measurement of fecal 5FU levels revealed detectable drug in patient stools, albeit with substantial interindividual variation (median: 0.08 μg/g stool) (Fig. 1E). Using solid culture conditions that better mimic the fecal solid microenvironment, levels as low as 0.03 μg/g solid medium were sufficient to completely inhibit *E. faecalis* growth (Fig. 1F; Fig. S1D), indicating that systemic 5FU therapy can reach inhibitory levels in the gut. Despite this, 5FU therapy did not alter the overall enterococcal abundance compared with healthy individuals (Fig. 1G). We therefore hypothesized that treatment may instead reshape the *E. faecalis* population at the strain level. To test this, we recovered *E.*

faecalis isolates from fecal samples of healthy individuals, patients receiving 5FU therapy, and those undergoing other drug treatments (Table S2). Based on the median fecal 5FU level (0.08 μg/g) and a stool density of approximately 1.07 g/mL[13], we derived an equivalent liquid concentration of 0.075 μg/mL. Isolates with 5FU MICs above this value were considered capable of surviving in the gut under therapy, whereas those with MICs below this value were not. Using this functional classification, we found that isolates with 5FU MIC > 0.075 μg/mL could be recovered from all three groups (Fig. 1H). However, the distribution of individual-level colonization patterns differed. 5FU-treated patients exhibited a higher proportion of individuals colonized exclusively by isolates with 5FU MIC > 0.075 μg/mL, accompanied by a corresponding reduction in mixed-colony carriers (both 5FU MIC > 0.075 μg/mL and 5FU MIC < 0.075 μg/mL clones) (Fig. 1H). These data suggest that naturally occurring 5FU-tolerant subpopulations are present in a subset of individuals. Upon 5FU treatment, selective pressure confers a growth advantage to these pre-existing tolerant strains, driving their clonal dominance within the detectable intestinal microbiota.

E. faecalis **metabolizes 5FU to promote its own tolerance**

Among isolates with MICs exceeding the 0.075 μg/mL threshold (Fig. 1H), we observed appreciable heterogeneity in their actual MIC values (Fig. 2A). This broad MIC distribution points to varying degrees of 5FU tolerance among naturally occurring subpopulations. To dissect the underlying basis, we selected 12 isolates recovered from a single 5FU-treated individual (#1) (Fig. 2A). Six of these isolates displayed MICs below the *in vitro* susceptibility breakpoint (0.19 μg/mL), whereas the other six exhibited higher MICs, exceeding 1 μg/mL (Fig. 2A). Accordingly, we operationally classified the former as a low-5FU-MIC *E. faecalis* (LM-*Efs*) lineage and the latter as a high-5FU-MIC *E. faecalis* (HM-*Efs*) lineage. HM-*Efs* isolates exhibited markedly elevated MIC values under both

aerobic and anaerobic culture conditions (Fig. 2B) and are therefore referred to hereafter as 5FU-resistant *E. faecalis* under our experimental conditions. Whole-genome sequencing of the 12 isolates from individual #1 revealed that the six LM-*Efs* isolates were genetically indistinguishable from one another, and the six HM-*Efs* isolates similarly displayed internal clonality (Fig. S2, A to C). Comparative analysis further showed that the LM-*Efs* and HM-*Efs* groups represent two distinct *E. faecalis* strains (or clonal lineages) (Fig. S2, B and C), rather than divergent subpopulations arising from a single strain. Scanning electron microscopy revealed that, unlike the rough-surfaced LM-*Efs* isolates, the HM-*Efs* isolates exhibited a smooth surface (Fig. 2C). This observation prompted us to ask whether 5FU might enter HM-*Efs* cells less efficiently. To test this, we measured intracellular 5FU concentrations after a 60-minute exposure to varying drug concentrations and found no appreciable difference between LM-*Efs* and HM-*Efs* (Fig. 2D). However, when cells were pulsed with 5FU for 60 mins and then transferred to drug-free buffer, intracellular 5FU declined more rapidly in HM-*Efs* than in LM-*Efs* over time (Fig. 2E), suggesting that enhanced metabolic degradation underlies the higher 5FU resistance of HM-*Efs*.

The PreT/A enzyme is known to metabolize 5FU in Gram-negative bacteria[11,14], but its presence in Gram-positive organisms has not been reported. A BLAST search of the LM-*Efs* and HM-*Efs* genomes using *E. coli* PreT/A sequences failed to identify homologs. However, structural prediction of all genes from both strains and subsequent comparison with the *E. coli* PreT/A structures led us to identify, in both LM-*Efs* and HM-*Efs*, two genes with marked structural similarity to PreA and one gene with marked similarity to PreT (Fig. 2F; Fig. S2D). The amino acid sequences of these three genes were identical between LM-*Efs* and HM-*Efs* (Fig. S2D). Database searches confirmed the presence of these PreT/A-like genes in other *E. faecalis* isolates as well (Fig. S2D). Notably, all

three *preT/A*-like genes were expressed at higher basal levels in HM-*Efs* than in LM-*Efs* (Fig. 2G). Moreover, upon 5FU exposure, two of these genes were significantly upregulated, and the induction was more pronounced in HM-*Efs* (Fig. 2G). Using all *E. faecalis* isolates recovered from both healthy individuals and 5FU-treated patients, we found that 5FU MICs correlated positively with *preT/A* expression levels, with strains exhibiting higher *preT/A* expression showing higher MICs (Fig. 2H). These findings demonstrate that *E. faecalis* possesses PreT/A-like enzymes capable of metabolizing 5FU, and that differential expression of these genes, both at baseline and in response to the drug, contributes to the varying levels of 5FU tolerance observed among strains.

5FU-resistant *E. faecalis* produces higher NADPH to alleviate oxidative stress

Besides inhibiting pyrimidine metabolism, 5FU also elevates bacterial ROS levels[15,16]. We found that 5FU markedly increased ROS production in LM-*Efs* but had no appreciable effect on ROS levels in HM-*Efs* (Fig. 3A). Notably, baseline ROS levels were substantially lower in HM-*Efs* than in LM-*Efs*. Under both aerobic and anaerobic conditions, HM-*Efs* maintained higher NADPH levels than LM-*Efs* (Fig. 3B). NADPH serves as the ultimate donor of reducing equivalents for the majority of ROS-detoxifying enzymes[17]. Treatment with 0.01 μg/mL 5FU decreased NADPH levels in both strains, while 0.03 μg/mL 5FU further reduced NADPH in LM-*Efs* but had little additional effect in HM-*Efs* (Fig. 3C), suggesting that HM-*Efs* utilizes its higher NADPH reserves to buffer against 5FU-induced oxidative stress. Consistent with this, HM-*Efs* exhibited greater tolerance to H_2O_2 than LM-*Efs* (Fig. S3A), indicating enhanced resistance to oxidative challenge.

To explore the basis for the elevated NADPH levels in HM-*Efs*, we first compared the proteomes of LM-*Efs* and HM-*Efs* (Table S3; Fig. 3D). Although

antioxidant enzymes SodB and GshR were upregulated in HM-*Efs*, the two primary NADPH-producing enzymes of the pentose phosphate pathway (PPP), Zwf and Pgl, were not significantly elevated (Fig. 3D), suggesting that increased NADPH synthesis capacity is not responsible. Comparative metabolomics revealed that many metabolites differentially abundant between the two strains mapped to pathways linked to wall teichoic acid (WTA) biosynthesis, including pentose and glucuronate interconversions, the PPP, pyrimidine metabolism, and amino sugar and nucleotide sugar metabolism (Table S4; Fig. 3, E to H). Among the most striking differences was CDP-ribitol, which was more than 250-fold lower in HM-*Efs* than in LM-*Efs* (Fig. 3I). CDP-ribitol is synthesized by TarI from CTP and D-ribitol 5-phosphate (Ribitol-5P), the latter generated by TarJ from D-ribulose 5-phosphate (Ribulose-5P) in a reaction that consumes NADPH (Fig. 3H)[18]. Ribulose-5P lies downstream of Zwf and Pgl in the PPP (Fig. 3H). Consistent with the depletion of CDP-ribitol, TarI protein levels were markedly reduced in HM-*Efs* (Fig. 3D). Genome comparison revealed that the *tarI* gene is entirely absent from the HM-*Efs* genome (Fig. S3B). This absence blocks the conversion of Ribitol-5P to CDP-ribitol, causing Ribitol-5P accumulation and product inhibition of TarJ[19,20], thereby reducing NADPH consumption at this step. Elevated levels of Ribulose-5P, ribose, and ribose-1-phosphate in HM-*Efs* support this model (Fig. 3, G and H), in which the diversion of PPP intermediates toward ribose and ribose-1-phosphate occurs once the route to CDP-ribitol is disabled. Metabolomic data also showed increased abundances of several NADPH precursors, including nicotinamide, NMN, NAD^+, and $NADP^+$, in HM-*Efs*, providing additional evidence for a heightened NADPH pool (Fig. S3, C and D). We also found the metabolites linked to the reversible reaction catalyzed by PreT/A. The abundance of dihydrouracil was higher in HM-*Efs* than in LM-*Efs*, whereas uracil (a structural analog of 5FU) was lower (Fig. S3E). This pattern is consistent with higher PreT/A activity in HM-*Efs*, leading to enhanced metabolic flux through this

enzyme and, consequently, greater 5FU metabolism.

CDP-ribitol is a key component of WTA in many Gram-positive bacteria. Because LM-*Efs*, but not HM-*Efs*, produces the CDP-ribitol, we hypothesized that its WTA content might be more vulnerable than that of HM-*Efs* to 5FU exposure, as 5FU-induced ROS elevation consumes NADPH, reducing the availability of this cofactor for TarJ and thereby limiting CDP-ribitol synthesis. Consistent with this model, 5FU treatment significantly reduced WTA levels in LM-*Efs* but had only a modest effect in HM-*Efs* (Fig. 3J). Collectively, these findings indicate that HM-*Efs* strains in this study have evolved, through genomic alterations, to minimize NADPH consumption by endogenous metabolic pathways, thereby maintaining a high NADPH pool that confers a survival advantage under oxidative stress.

5FU-resistant *E. faecalis* exhibits enhanced resistance to clinical antibiotics

Genomic analysis of antibiotic resistance genes (ARGs) in LM-*Efs* and HM-*Efs* revealed that HM-*Efs* harbors a greater diversity and higher total number of ARGs (Table S5; Fig. 4A). Specifically, HM-*Efs* carries more genes associated with tetracycline resistance, correlating with its higher MICs against both tigecycline and tetracycline compared with LM-*Efs* (Fig. 4B). Additionally, HM-*Efs* possesses ARGs for linezolid and chloramphenicol, consistent with its elevated MICs against these agents (Fig. 4, A and B). When we extended our susceptibility testing to other antibiotic classes, we found that HM-*Efs* also exhibited higher MICs against cephalosporins and fluoroquinolones (Fig. 4, B and C). For levofloxacin, the MIC for HM-*Efs* was only 2.5-fold higher than for LM-*Efs*; however, for Cefuroxim (CFX) and cefotaxime (CTX), the MICs for HM-*Efs* exceeded those for LM-*Efs* by more than 15-fold (Fig. 4B).

No canonical resistance genes for these two antibiotic classes were identified in the HM-*Efs* genome, and plasmid conjugation from HM-*Efs* into LM-*Efs* failed to transfer cephalosporin resistance (Fig. 4D; Fig. S4, A to C), indicating that the observed phenotype is unlikely mediated by plasmid-borne horizontally acquired elements. *E. faecalis* exhibits intrinsic resistance to cephalosporins through its low-affinity class B penicillin-binding protein 4 (PBP4), although PBP4-mediated resistance requires functional partners among class A PBPs[21,22]. While PBP4 expression levels were comparable between LM-*Efs* and HM-*Efs*, the latter displayed markedly higher transcript levels of *pbp1b*, *pbp2a*, and *pbp2b* (Fig. 4E), likely accounting for its enhanced cephalosporin resistance. Strikingly, exposure to 5FU upregulated *pbp1b*, *pbp2a*, and *pbp2b* in both strains, and the induced expression of pbp2b remained higher in HM-*Efs* than in LM-*Efs* (Fig. 4F). Together, these findings demonstrate that the 5FU-resistant *E. faecalis* strains identified in this study possess a broader and more potent resistance phenotype against multiple clinically relevant antibiotics. They also raise the concern that 5FU therapy may inadvertently promote the expansion and colonization of such multidrug-resistant *E. faecalis* populations.

5FU-resistant *E. faecalis* exhibits enhanced virulence in mice and outcompetes susceptible strains under 5FU exposure

We then asked whether LM-*Efs* and HM-*Efs* differ in their pathogenic potential. Following intravenous infection in mice, HM-*Efs* caused mortality in a subset of animals at a dose at which all mice infected with LM-*Efs* survived (Fig. 5A). Organ bacterial burdens mirrored this difference, with HM-*Efs* replicating in the liver, spleen, and kidneys to levels 10- to 100-fold higher than those seen with LM-*Efs* (Fig. 5B). Notably, the tissue burdens achieved by HM-*Efs* were comparable to those of V583 (Fig. 5B), a hospital-associated, multidrug resistant *E. faecalis* isolate from a chronically infected patient[23]. These results indicate that HM-*Efs* is more virulent than LM-*Efs*.

Because both strains were recovered from the same patient, we asked whether they interact competitively. In rich medium, HM-*Efs* reached a higher final OD_{600} than LM-*Efs* when grown alone (Fig. 5C). However, when the two strains were co-cultured starting from a 1:1 ratio, the growth curve resembled that of LM-*Efs* alone (Fig. 5C), suggesting that LM-*Efs* might suppress HM-*Efs*. To test this directly, we exploited differential antibiotic resistance. HM-*Efs*, but not LM-*Efs*, grows on plates containing 10 μg/mL chloramphenicol. To selectively enumerate LM-*Efs*, we generated a spontaneous rifampicin resistant derivative of this strain (Fig. S4A); rifampicin resistance did not alter its growth. Using this differential plating strategy, we found that after 8 h of co-culture starting from a 1:1 inoculum, LM-*Efs* proliferated steadily whereas HM-*Efs* declined under both aerobic and anaerobic conditions (Fig. 5D; Fig. S5A). This indicates that LM-*Efs* actively inhibits HM-*Efs*. Diluted conditioned medium from LM-*Efs* cultures reproduced this inhibitory effect (Fig. 5E), suggesting that the inhibition is mediated by secreted factor(s).

These findings raised a paradox: if LM-*Efs* suppresses HM-*Efs*, how did both strains coexist in the same patient at comparable numbers? We hypothesized that 5FU, to which LM-*Efs* is sensitive, might relieve this suppression. To test this, we added 0.2 μg/mL 5FU to monocultures and co-cultures of the two strains. This concentration completely inhibited LM-*Efs* growth but had no effect on HM-*Efs* (Fig. 5F). In co-culture with 5FU, little growth was observed until after 10 h (Fig. 5F). Plating the resulting cultures on selective antibiotics revealed that only HM-*Efs* survived; no LM-*Efs* colonies were recovered (Fig. 5G; Fig. S5B). Thus, 5FU eliminates the competitive suppression imposed by LM-*Efs*, allowing the more virulent HM-*Efs* to proliferate. Together, these results demonstrate that HM-*Efs* is more virulent than LM-*Efs* and that, under normal conditions, LM-*Efs* suppresses its growth. However, 5FU treatment removes

this suppression, enabling the expansion of the hypervirulent strain and creating opportunities for subsequent infection or transmission.

Competitive release of 5FU-resistant *E. faecalis* during 5FU chemotherapy in mice

To directly test whether LM-*Efs* and HM-*Efs* compete *in vivo* and whether 5FU relieves this competition, we established a cage-controlled colonization model in C57BL/6J mice (Fig. 6A; Fig. S6). Mice were organized at the cage level (five mice per cage), including a PBS-treated control group without antibiotic exposure and multiple antibiotic-pretreated groups subjected to distinct colonization conditions, including single-strain and sequential colonization. Following antibiotic-mediated depletion of the gut microbiota, confirmed by a marked reduction in total bacterial load after two weeks (Fig. S6A), mice were colonized with either LM-*Efs* or HM-*Efs* by oral gavage (Fig. 6A). Both strains achieved comparable colonization levels (Fig. 6, B and C; Fig. S6B). We then introduced the opposite strain into already colonized mice (cross-colonization) to assess competitive outcomes (Fig. 6A). Regardless of whether HM-*Efs* was introduced into LM-*Efs*-colonized mice or LM-*Efs* into HM-*Efs*-colonized mice, fecal shedding of HM-*Efs* was significantly lower than in mice colonized with HM-*Efs* alone (Fig. 6, B and C; Fig. S6C). In contrast, LM-*Efs* shedding was unaffected by the presence of HM-*Efs* (Fig. 6, B and C; Fig. S6C). These results demonstrate that LM-*Efs* actively suppresses HM-*Efs* in the gut.

We next asked whether 5FU treatment, at a dose equivalent to that used in patients, could reverse this suppression (Fig. 6A). In both cross-colonization settings, 5FU administration markedly reduced LM-*Efs* shedding while allowing HM-*Efs* to rebound (Fig. 6, B and C; Fig. S6D). Thus, 5FU therapy selectively suppresses the growth of less tolerant strains such as LM-*Efs*, while exerting no inhibitory effect on highly 5FU-resistant strains like HM-*Efs*. These resistant

strains possess a multifaceted fitness advantage, including enhanced capacity to resist oxidative stress, broader and stronger antibiotic resistance profiles, and increased virulence *in vivo*. The combination of 5FU-driven selection and the intrinsic pathogenic traits of HM-*Efs* creates a concerning scenario in which therapy inadvertently promotes the expansion and dissemination of a more virulent, multidrug-resistant *E. faecalis* subpopulation, with potential implications for transmission in healthcare and community settings.

Discussion

Chemotherapy-induced gut injury and dysbiosis are well recognized, and microbiota changes can contribute to mucositis, inflammation, and infectious complications[24,25]. Yet community profiling often collapses within-species heterogeneity, despite evidence that gut species frequently comprise multiple strains and undergo rapid within-host evolutionary and ecological turnover[6,26-28]. Our results highlight the clinical relevance of this resolution gap, as 5FU emerged as the strongest broad-spectrum antibacterial *in vitro* across a curated panel of FDA-approved anticancer agents and was particularly potent against Gram-positive organisms, including *E. faecalis*. In patients receiving standard intravenous 5FU, measurable fecal drug levels reached concentrations that fully inhibit susceptible *E. faecalis* under fecal-like solid conditions, yet total enterococcal abundance remained unchanged. Instead, 5FU therapy shifted colonization architecture toward pre-existing tolerant lineages, reducing mixed carriage and enriching clones able to survive the inferred intestinal exposure. These findings formalize a simple point with broad implications: systemic chemotherapy can impose strong, clinically meaningful selection on gut pathobionts at the strain level even when species-level abundance metrics appear stable.

Fluoropyrimidines exemplify pharmacomicrobiomics. Gut bacteria can

metabolize 5FU to DHFU, an inactive product that mirrors a major host clearance route. In *Escherichia coli*, the bacterial *preTA* operon is necessary and sufficient for this inactivation and measurably alters fluoropyrimidine bioavailability and antitumor efficacy in mice[10]. Recent longitudinal human work further indicates that *preTA*-associated features can increase during fluoropyrimidine therapy and correlate with clinical treatment parameters, underscoring translational relevance[29]. Building on this framework, our data extend metabolic detoxification to a Gram-positive pathobiont. High-level 5FU-resistant *E. faecalis* did not show reduced intracellular 5FU accumulation after initial exposure, but displayed more rapid intracellular drug loss in pulse-chase assays, implicating enhanced degradation rather than restricted uptake. Although canonical Gram-negative PreT/A sequence homologs were not detectable by sequence-based BLAST searches, proteome-wide AlphaFold3 structure prediction followed by Foldseek-based structural homology search uncovered cryptic PreT/A-like proteins, whose basal and drug-induced expression was elevated in the resistant lineage. Across isolates, *preT/A*-like expression correlated positively with 5FU MIC, supporting an expression-tuned detoxification axis that stratifies strain fitness under therapy.

Beyond disrupting nucleotide metabolism, 5FU can impose oxidative stress in bacteria, including ROS-associated antibacterial effects observed under inhibitory exposure[16,30]. Oxidative stress is also a pervasive challenge during infection, as host phagocytes deploy ROS in the oxidative burst[31], and successful pathogens evolve strategies to survive or blunt ROS-mediated restriction[32]. Consistent with this broader biology, *E. faecalis* oxidative stress tolerance has been repeatedly linked to virulence potential and survival during dissemination from the gut to extraintestinal sites[33]. In our study, highly 5FU-resistant lineages maintained lower basal ROS and higher NADPH pools across conditions, and showed enhanced tolerance to exogenous oxidative

challenge. This alignment between drug resistance and redox robustness suggests that therapy selects not only for lineages that can detoxify the drug but also for lineages that can buffer the collateral oxidative stress associated with fluoropyrimidine exposure and host-associated inflammatory environments[34]. NADPH is a central bacterial reducing equivalent that underwrites anabolic pathways and antioxidant systems required to detoxify ROS and restore redox homeostasis[34]. The metabolomic signature of the high-resistance lineage supports a “NADPH economy” model linked to cell-envelope metabolism. Loss of *tarI* coincided with profound depletion of CDP-ribitol, and TarJ functions as an NADPH-dependent reductase in the CDP-ribitol/WTA precursor pathway[20]. By curtailing NADPH-consuming flux into this branch, the resistant lineage can plausibly preserve reducing power for ROS buffering, consistent with general principles of microbial oxidative-stress adaptation[35].

Ecologically, our results support competitive release, whereby 5FU removes a susceptible strain that otherwise suppresses a resistant competitor, a mechanism long discussed in resistance emergence when treatment disproportionately harms sensitive types and thereby relaxes competitive constraints[36]. In co-culture, the susceptible lineage actively inhibited the resistant lineage, and diluted conditioned medium reproduced inhibition, implicating secreted antagonist(s) whose identity remains unspecified. Enterococci are well known to secrete bacteriocins (enterocins) and related antimicrobials that mediate inter-strain competition, offering a plausible mechanistic class for the observed conditioned-medium effect without over-committing to a specific molecule[37]. Under 5FU exposure that extinguished the susceptible lineage, inhibition was abrogated and only the resistant lineage survived. *In vivo*, the resistant lineage was constrained at baseline but rebounded when 5FU suppressed the susceptible competitor during cross-colonization. Critically, the released lineage carried broader antibiotic

resistance and showed elevated transcription of class A PBPs that participate in enterococcal intrinsic β-lactam and cephalosporin resistance networks, paralleling increased cephalosporin MICs[21,22]. This lineage also exhibits enhanced virulence in systemic murine infection, consonant with the broader capacity of enterococci to couple stress tolerance, resistance, and pathogenicity[38].

These results have several translational implications. First, they argue for incorporating strain-resolved microbiome measurements into oncology-associated infection risk models, because species-level abundance may be insufficient to detect hazards that matter clinically[39]. Second, they suggest that microbial xenometabolic capacity, as reflected in PreT/A-like expression and associated metabolic outputs, could serve as a functional biomarker of the likelihood that therapy will enrich resistant lineages. Emerging cohort studies during fluoropyrimidine therapy have begun to link *preTA*-associated features with drug response and dose adjustment, underscoring the feasibility of such an approach[40]. Third, they motivate “ecological management” strategies in cancer care that aim to anticipate and steer microbiota dynamics, for example through monitoring, targeted decolonization approaches, or microbiota-preserving practices[41]. Key limitations include the use of fecal drug concentrations as proxies for spatially heterogeneous intestinal exposures and the need for targeted genetic tests to establish causal links connecting detoxification and NADPH/redox economy circuits to resistance and virulence phenotypes[42]. Broader validation across patient populations, treatment regimens and microbial backgrounds will also be required to define the generality of chemotherapy-driven competitive release[26,43].

Materials and Methods

Ethnic statement

The Shenzhen Bay Laboratory Medical Ethical Committee reviewed, approved, and supervised the protocol (No. YL 2024-010) used for all experiments utilizing blood from human volunteers and informed consent forms were obtained from all participants. Animal research was performed in accordance with institutional guidelines following experimental protocol review, approval, and supervision by the Institutional Animal Care and Use Committee at the Shenzhen Bay Laboratory (Approval No. AECXH202302). Experiments with pathogenic bacteria were performed in biosafety level 2 (BSL2)/animal BSL2 (ABSL2) containment upon review by Shenzhen Bay Laboratory Institutional Biosafety Committee.

Bacterial strains and growth conditions.

*Salmonella t*yphimurium (*St*) was from laboratory stocks. *Klebsiella pneumonia* MGH78578 (*Kp*), *Acinetobacter baumannii* ATCC17978 (*Ab*), and *Pseudomonas aeruginosa* 278523 (*Pa*) were gifts from the laboratory of Prof. Xin Ding, Sun Yat-sen University. *Escherichia coli* BW25113(*Ec*) was from laboratory stocks. *Enterococcus faecium* D5726 (*Efc*) and *Enterococcus faecalis* strains (*Efs*) were gifts from the laboratory of Prof. Hua Zhou, Zhejiang University. *Staphylococcus epidermidis* 1471 (*Se*), *Listeria monocytogenes* EGDe (*Lm*), *Corynebacterium diphtheria* C7(*Cd*), *Bacillus subtilis* PY79(*Bs*), and *Staphylococcus aureus* Newman (*Sa*) were from laboratory stocks. All strains were routinely cultured in Tryptic Soy Broth (TSB) medium at 37°C.

Anti-tumor compound library screen.

An FDA-approved anti-tumor compound library containing 217 drugs (Table S1) was purchased from TargetMol. The Gram-negative bacterium *E. coli* BW25113 and the Gram-positive bacterium *S. aureus* Newman were used for screening. Briefly, single colonies were inoculated into TSB and cultured overnight. Bacterial cells were harvested, washed three times with sterile saline, and

resuspended. Using an ECHO 650 acoustic liquid handler, the bacterial suspensions were transferred into 384-well plates (Corning 3765) containing TSB medium with serially diluted compounds (final concentrations: 2 μM, 20 μM, 200 μM). The final bacterial dilution in each well was 1:1000. Bacterial growth was monitored by measuring OD_{600} every 15 min for 24 h at 37°C with continuous orbital shaking (medium speed) in a BioTek microplate reader. Wells containing medium with compound but no bacteria served as blanks. The area under the curve (AUC) for growth was calculated. The AUC for bacteria grown in compound-free medium was defined as 100%, and the inhibition rate for each compound was calculated as: (1 - (AUC_compound / AUC_control)) × 100%.

Minimum Inhibitory Concentration (MIC) determination.

MICs were determined using the broth microdilution method according to CLSI guidelines[44]. Briefly, bacteria from overnight cultures were adjusted to approximately 5×10^5 CFU/mL in indicated medium. Antimicrobial agents were serially diluted two-fold in 96-well plates. An equal volume of the adjusted inoculum was added to each well. The plates were incubated at 37°C for 16-18 h. The MIC was defined as the lowest concentration of antimicrobial agent that completely inhibited visible growth. The following antimicrobial agents were used in this study: tigecycline (TIG), linezolid (LIN), levofloxacin (LEV), cefuroxime (CFX), cefotaxime (CTX), chloramphenicol (CHL), tetracycline (TET), cefpirome (CPB), moxifloxacin (MLFX), daptomycin (DATO), kanamycin (KAN), gentamicin (GEN), neomycin (NEO), spectinomycin (SPEC), clarithromycin (CT), clindamycin (CLIN), rifampin (also known as rifampicin, RIF), erythromycin (ERM), metronidazole (MET), vancomycin B (VAN), and polymyxin B (PB). All antibiotic stock solutions were prepared according to the CLSI guidelines, filter-sterilized through 0.22 μm membranes, and stored at -20°C until use. Working concentrations were freshly prepared prior to each experiment. All experiments were performed in biological triplicate.

Growth curve analysis.

A single colony of indicated bacterial strain was inoculated into 3 mL rich medium and cultured overnight. The overnight culture was diluted 1:100 into fresh medium (or medium containing specified reagents) in a 96-well plate (200 μL per well). Growth was monitored by measuring OD_{600} every 15 min for 16 h at 37°C with continuous orbital shaking in a BioTek microplate reader. To minimize evaporation, the outer wells of the plate were filled with sterile medium or water.

Quantification of 5FU in human stool samples.

Fecal samples stored at -80°C were thawed on ice. Approximately 0.1 g of feces was weighed. Metabolites were extracted by adding 1 mL of extraction solvent (methanol:acetonitrile:water, 2:2:1, v/v), followed by vortexing for 30 s, flash-freezing in liquid nitrogen for 1 min, and ultrasonication for 5 min. This freeze-thaw-sonicate cycle was repeated three times. After incubation at -20°C for 1 h, samples were centrifuged at 13,000 g for 15 min at 4°C. The supernatant was transferred to a new tube and dried under vacuum at 4°C. The dried extract was reconstituted in 1 mL of solvent (methanol:acetonitrile:water, 2:2:1, v/v), centrifuged, and filtered through a 0.22 μm organic filter. Analysis was performed using a SCIEX QTRAP 6500+ LC-MS/MS system with a C18 column in negative ion mode. The optimized multiple reaction monitoring (MRM) transitions for 5FU were: m/z 129 → 85.9, 129 → 42, and 129 → 59.2. A standard curve was constructed using 5FU standards at concentrations of 0.001, 0.003, 0.006, 0.012, 0.025, and 0.05 μg/mL[45,46]. Fecal 5FU concentrations were calculated based on the integrated peak area relative to the standard curve.

Isolation and identification of bacteria from human feces.

Selective isolation of *E. faecalis* was performed using Enterococcus agar. Fecal samples (0.01 g) were homogenized in 100 μL PBS, filtered, and serially diluted. Appropriate dilutions were plated on the selective media and incubated at 37°C overnight. Single colonies with distinct morphologies were picked, purified by re-streaking, and cultured overnight in LB broth. Genomic DNA was extracted using a bacterial genomic DNA extraction kit. The 16S rRNA gene was amplified using universal primers 27F (AGAGTTTGATCCTGGCTCAG) and 1492R (TACGGTTACCTTGTTACGACTT). PCR products were Sanger sequenced. For isolates identified as *Enterococcus*, species differentiation between *E. faecalis* and *E. faecium* was performed by PCR targeting the *ddl* gene with specific primers (ddl-F: ATCAAGTACAGTTAGTCTT; ddl-R: ACGATTCAAAGCTAACTG) [47]. All identifications were further confirmed by matrix-assisted laser desorption/ionization time-of-flight (MALDI-TOF) mass spectrometry following the manufacturer's instructions.

Bacterial inhibition assay with fecal-relevant 5FU concentrations.

Bacterial overnight cultures were diluted to OD600 ≈ 0.2, washed, and resuspended in saline. After serial dilution, bacteria were plated on Tryptic Soy Agar (TSA) plates supplemented with 5FU at concentrations (0.01, 0.03, 0.05, 0.08 μg/g) designed to mimic the median and range of 5FU concentrations measured in patient stool samples. Plates (90 mm diameter containing 15 g medium) were incubated at 37°C, and colony-forming units (CFU) were enumerated.

Quantitative real-time PCR (qRT-PCR) for Enterococcus quantification.

Total RNA was isolated using a phenol-chloroform-based method. Cultures were harvested at specified growth phases. Cell pellets were resuspended in 1 mL of TSM buffer (10mM Tris-HCl, pH 7.5, 500 mM sucrose, 10 mM $MgCl_2$) containing 1 mg/mL lysozyme and incubated at 37°C for 30 min to digest the

cell wall，centrifugation at 12,000 × g for 15 min at 4°C. Following digestion, 1 mL of TRIzol reagent was added directly to the sediment. After thorough mixing, phase separation was achieved by adding 200 μL chloroform, vigorous shaking, and centrifugation at 12,000 × g for 15 min at 4°C. The aqueous phase was transferred, and RNA was precipitated with 0.5 volumes of isopropanol, washed with 75% ethanol, and dissolved in DEPC-treated water. Residual DNA was removed using the TURBO DNA-free™ Kit. cDNA was synthesized from 500 ng RNA using the iScript™ cDNA Synthesis Kit. qPCR was performed using iQ™ SYBR® Green Supermix on a CFX96 Real-Time System.

Anaerobic MIC determination for *E. faecalis*.

MIC determination under strict anaerobic conditions was performed according to CLSI guidelines. All media and plates were pre-reduced in an anaerobic chamber (BACTRON 300-2, SHELLAB) for at least 24 h prior to use. *E. faecalis* strains were cultured anaerobically in TSB. The broth microdilution method was performed inside the anaerobic workstation. The MIC was read after 16 h of incubation at 37°C, with optical density measured at 600 nm for confirmation.

Determination of intracellular 5FU concentration in *E. faecalis*.

Overnight cultures of *E. faecalis* were harvested, washed with PBS, and resuspended in PBS to OD600 = 1.0. A 10 mL aliquot of the cell suspension was incubated with indicated concentrations of 5FU for 1 h at 37°C. Bacterial cells were harvested, washed three times with cold PBS, and quenched with 1 mL cold methanol. After centrifugation, the pellet was resuspended in 400 μL water and digested with lysozyme (3 mg/mL) at 37°C for 30 min. A mixture of methanol, acetonitrile and water (2:2:1, v/v) was added, followed by ultrasonication. The supernatant was collected after centrifugation, dried under vacuum at 4°C, and reconstituted in 200 μL of mixture. After a final centrifugation, the supernatant was filtered and analyzed by LC-MS/MS as

described for fecal samples. A standard curve was used for quantification, with a 0.001 μg/mL standard run concurrently.

Scanning Electron Microscopy (SEM) of *E. faecalis*.

E. faecalis cultures (OD600 = 1.0) were harvested, washed with PBS, and fixed with 2.5% glutaraldehyde at 4°C overnight. Samples were post-fixed with 1% osmium tetroxide, dehydrated through a graded ethanol series, critical-point dried, and sputter-coated with gold. Images were acquired using a scanning electron microscope[48].

Whole-genome sequencing of *E. faecalis*.

Genomic DNA was extracted from *E. faecalis* strains and subjected to high-throughput sequencing using both Illumina short-read and Oxford Nanopore long-read platforms to achieve high coverage depth. Hybrid genome assembly was performed by integrating short- and long-read datasets to generate complete circular genomes. Long reads were used to resolve repetitive regions and structural complexities that typically hinder assembly continuity, while short reads were applied for base-level error correction to improve sequence accuracy. This combined approach enabled the reconstruction of gap-free, closed genomes. Bioinformatic analysis, including *de novo* genome assembly, genome annotation, and variant calling, was conducted by Guangdong Magigene Biotechnology Co.,Ltd. (Guangzhou, China).

Structural homology modeling of *E. faecalis* PreA/T proteins.

To identify proteins in the LM- and HM-*Efs* genome with structural similarity to the PreA and PreT proteins, monomeric structural models were generated using AlphaFold 3[49] for all entries in both the LM- and HM-*Efs* genome and the two query protein sets. For each entry, the top-ranked model and five additional sampled conformations were retained. The predicted structures of the two

query sets were then searched against the LM- and HM-*Efs* predicted structure library using Foldseek[50]. Hits were prioritized by bit score, alignment length, and sequence identity. Redundant matches arising from alternative sampled conformations were resolved by retaining only the highest-scoring record for each unique query-target pair.

Proteomic analysis of *E. faecalis*.

E. faecalis strains were inoculated into TSB and cultured overnight at 37°C with shaking at 220 rpm to reach the stationary phase. Bacterial cells were harvested by centrifugation at 7,000×g for 3 min. The pellet was washed once and resuspended in sterile saline, followed by a second centrifugation under the same conditions. The washed cell pellet was resuspended in ultrapure water, and the optical density at 600 nm (OD_{600}) was adjusted to 1.0. A 10 mL aliquot of this adjusted suspension was centrifuged at 7,000×g for 3 min. The supernatant was discarded, and the pellet was resuspended in 100 μL of ultrapure water. For cell lysis, lysozyme was added to the suspension, followed by incubation at 37°C for 30 min. Then, 900 μL of ice-cold urea lysis buffer (8 M urea, 75 mM NaCl, 50 mM Tris-HCl pH 8.0, 1 mM EDTA) was added to the suspension, supplemented with protease inhibitors (1 mM PMSF), phosphatase inhibitors (Phosphatase Inhibitor Cocktail 2), and 5 mM iodoacetamide, and incubated for 30 min on ice. The lysate was clarified by centrifugation at 20,000×g for 10 min at 4°C. Protein concentration was determined using a bicinchoninic acid (BCA) assay. For protein digestion, disulfide bonds were reduced with 50 mM dithiothreitol at 60°C for 45 min, followed by alkylation with 100 mM iodoacetamide in the dark for 1 h. The sample was then diluted 4-fold with 50 mM Tris-HCl (pH 8.0) to reduce the urea concentration to 2 M. Trypsin was added at an enzyme-to-substrate ratio of 1:50 (w/w), and digestion proceeded overnight (12-16 h) at 37°C with gentle shaking. The digestion was stopped by acidifying the peptide mixture with formic acid to a final

concentration of 1% (v/v). Precipitated urea was removed by centrifugation at 2,000×g for 5 min. For a typical sample containing 10-30 μg of peptides, desalting was performed using a Pierce C18 Spin Column. The column was activated with 200 μL of 50% acetonitrile (centrifuged at 1,500×g for 1 min, repeated five times) and equilibrated twice with 200 μL of 0.1% trifluoroacetic acid (TFA). The acidified peptide sample was loaded onto the column and centrifuged. The bound peptides were washed four times with 200 μL of 0.1% TFA. Peptides were eluted with two aliquots of 100 μL of 80% acetonitrile. The combined eluents were dried in a vacuum concentrator. The dried peptide sample was reconstituted in 20 μL of 0.1% formic acid. Peptide concentration was measured by absorbance at 205 nm using a Nanodrop spectrophotometer and adjusted to 250 ng/μL. Finally, the sample was centrifuged at 14,000×g for 5 min, and the supernatant was transferred to a mass spectrometry vial for analysis. Peptides were desalted and analyzed by liquid chromatography-tandem mass spectrometry (LC-MS/MS) on a Q Exactive HF-X mass spectrometer coupled to an EASY-nLC 1200 system. Data were processed using MaxQuant software for identification and label-free quantification[51,52].

Metabolomic analysis of *E. faecalis*.

E. faecalis strains were inoculated into TSB and cultured overnight at 37°C with shaking at 220 rpm to reach the stationary phase. Bacterial cells were harvested by centrifugation at 7,000×g for 3 min. The pellet was washed once and resuspended in sterile saline, followed by a second centrifugation under the same conditions. The washed cell pellet was resuspended in ultrapure water, and the optical density at 600 nm (OD_{600}) was adjusted to 1.0. A 10 mL aliquot of this adjusted suspension was centrifuged at 7,000×g for 3 min. The supernatant was discarded, and the pellet was resuspended in 400 μL of ultrapure water. For cell lysis, lysozyme was added to the suspension, followed by incubation at 37°C for 30 min. The lysate was then subjected to ultrasonic

disruption (100 W, 5 min). Subsequently, 800 μL of methanol and 800 μL of acetonitrile were added to the sample. After thorough mixing, the solution was centrifuged at 12,000×g. The resulting supernatant was collected and lyophilized. The dried material was reconstituted in a resuspension solvent (methanol:acetonitrile:water, 2:2:1, v/v/v) with the aid of sonication for 15 min. The final sample was obtained by centrifugation to collect the supernatant for subsequent analysis. The extract was dried and reconstituted for LC-MS analysis on a Q Exactive HF-X mass spectrometer. Data were analyzed using Compound Discoverer and MetDNA[53].

Measurement of intracellular NADPH levels under aerobic and anaerobic conditions.

E. faecalis strains were grown to OD_{600} = 0.8 under aerobic or anaerobic conditions. Cells from 10 mL culture were harvested, washed, and lysed. For some experiments, metabolites were first extracted with methanol/acetonitrile before NADPH measurement. Intracellular NADPH concentration was determined using a commercial NADP/NADPH Assay Kit (Beyotime, S0179) following the manufacturer's protocol. Protein concentration was determined and used to normalize NADPH levels.

Measurement of intracellular ROS by flow cytometry.

E. faecalis cultures were grown to mid-log phase (OD_{600} ≈ 0.6). Carboxy-H_2DCFDA (10 μM final concentration) was added and incubated for 30 min at 37°C in the dark. Cells were washed twice with PBS and resuspended. Fluorescence was measured using a BD FACSC flow cytometer (excitation 488 nm, emission 530/30 nm). Data from 10^5 events were collected, and the median fluorescence intensity in the FL1 channel was used to quantify ROS levels. Unstained cells served as autofluorescence controls[54].

Extraction and analysis of wall teichoic acid (WTA).

WTA was extracted from *E. faecalis* as described previously with modifications[55]. Cells from a 30 mL culture (OD600 = 1.0) were harvested, washed, and boiled in 4% SDS. After washing, the pellet was digested with protease K. Following further washes, WTAs were released by hydrolysis in 0.1 M NaOH overnight at room temperature. The supernatant containing WTAs was neutralized. WTA samples were separated by SDS-PAGE, stained with 1 mg/mL Alcian Blue for 20 min, washed, and then visualized by silver staining using a commercial kit (Bio-Rad).

Conjugation assay.

The plasmid conjugation assay was performed as described previously[56]. Briefly, overnight cultures of the donor strain (LYT-5FU-R, carrying a chloramphenicol resistance plasmid) and the recipient strain (LYT-5FU-S, rifampicin-resistant) were diluted 1:100 in fresh TSB (donor with chloramphenicol). After growth to OD_{600} 0.2-0.6 (donor) and OD_{600} 0.1-0.2 (recipient), cultures were mixed at a 1:10 donor-to-recipient ratio, pelleted, and resuspended in 100 µL TSB. The cell mixture was spotted onto a TSA plate and incubated aerobically at 37°C for 20 h. The mating spot was resuspended, diluted, and plated on TSA containing rifampicin and chloramphenicol to select for transconjugants. Putative transconjugants were confirmed by PCR.

***E. faecalis* mouse infection model.**

Female CD1 mice (5-6 weeks old) were used. *E. faecalis* was grown to OD_{600} = 0.6, washed, and resuspended in sterile PBS at 2×10^9 CFU/mL. Mice were anesthetized with isoflurane and inoculated via retro-orbital injection with 100 µL of bacterial suspension or PBS (control). Body weight and survival were monitored daily for 7 days. Moribund mice or survivors at the experimental endpoint were euthanized. Heart, spleen, kidneys, and liver were aseptically

collected, weighed, homogenized, serially diluted, and plated on TSA to determine bacterial loads (CFU/g of tissue).

Inhibition assay with culture supernatant from 5FU-sensitive *E. faecalis*.
Overnight cultures of 5FU-sensitive and -resistant *E. faecalis* were centrifuged. The supernatants were filter-sterilized (0.22 μm) and stored at -80°C. The inhibitory effect of the supernatant from the sensitive strain on the resistant strain was tested using a broth microdilution method in 96-well plates. Growth was monitored by OD_{600} measurement.

Rifampicin passaging of LM-*Efs*.
An overnight culture of a 5FU-sensitive *E. faecalis* strain was diluted 1:9 into fresh TSB containing rifampicin at 1/2 MIC (0.05 μg/mL) and incubated statically at 37°C for 12 h. This passage was repeated every 12 h. The MIC of the passaged strain to 5FU was determined every 5 passages.

***In vitro* competition assay.**
Overnight cultures of a LM-*Efs* strain (marked with rifampicin resistance) and a HM-*Efs* strain were washed and mixed at a 1:1 cell ratio. The mixed inoculum was diluted 1:1000 into fresh TSB and incubated at 37°C. Samples were taken at 0 h and 8 h, serially diluted, and plated on TSA plates with no antibiotic, rifampicin (to select for the sensitive strain), or chloramphenicol (to select for the resistant strain, if applicable). Colony counts were used to calculate the proportion of each strain over time.

***In vivo* competition assay in a mouse colonization model.**
Female C57BL/6 mice (5-6 weeks old, n=4 per group) were used. To deplete the indigenous gut microbiota, mice received antibiotics in drinking water for two weeks: streptomycin (0.2 g/L) and spectinomycin (0.05 g/L) in week 1,

followed by kanamycin (0.5 g/L) and erythromycin (0.5 g/L) in week 2[57,58]. Successful depletion was confirmed by fecal plating. Mice were then orally gavaged with 200 μL of bacterial suspension (2×10^8 CFU) containing specified strains (LM-*Efs* and/or HM-*Efs*) twice a week for 4 weeks, with or without concomitant 5FU administration. Control mice received PBS. Fecal samples were collected regularly, homogenized, diluted, and plated on selective media to quantify *E. faecalis* colonization levels. Successful colonization was defined as a fecal load ≥ 10^7 CFU/g maintained for 7 days.

Statistical analysis

Data are presented as mean ± SEM. Statistical analyses were performed according to the experimental design as follows: comparisons between two groups were conducted using unpaired, two-tailed Student's t tests; comparisons among multiple groups under a single factor were analyzed by one-way analysis of variance (ANOVA) followed by appropriate multiple comparisons testing; and experiments involving two independent variables were evaluated using two-way ANOVA with multiple comparisons. Survival distributions were analyzed using the log-rank (Mantel-Cox) test. All analyses were carried out using Prism 10 (GraphPad Software). A P value of less than 0.05 was considered statistically significant.

Acknowledgement

We thank the Biosafety Level 2 (BSL-2) and Animal Biosafety Level 2 (ABSL-2) Laboratories of the Institute of Infectious Diseases, Shenzhen Bay Laboratory, for their support and assistance during this research.

Funding

Guangdong Pearl River Funding 2023QN10Y181 (XC); National Natural Science Foundation of China 32571106 (XC); National Natural Science

Foundation of China: 82371836 (XC); National Key R&D Program of China 2025YFA0923000 (CW); Guangdong Provincial Key R&D Program 2024B1111150001 (CW).

Author contributions

Conceptualization: XC and JY; Methodology: YJ, DW, YX, BC, and QT; Validation: YJ, DW, YX, and BC; Investigation: YJ, DW, BC, and YX; Resources: YJ, DW, YX, WC, and XL; Visualization: JY, DW, BC, QT, and XC; Funding acquisition: XC and CW; Project administration: JY, XC, and XL; Supervision: XC; Writing-original draft: YJ and XC; Writing-review & editing: YJ, XC, CW, and XL.

Competing interests

Authors declare that they have no competing interests.

Data and materials availability

All data are available in the main text or the supplementary materials. The raw sequence data reported in this paper have been deposited in the Genome Sequence Archive (Genomics, Proteomics & Bioinformatics 2025) in National Genomics Data Center (Nucleic Acids Res 2025), China National Center for Bioinformation / Beijing Institute of Genomics, Chinese Academy of Sciences. The raw genomics data are available under the accession number CRA036910 (preview link: https://ngdc.cncb.ac.cn/gsa/s/P9h59049). The raw proteomic and metabolomic data are available under the accession numbers OMIX015923 (preview link: https://ngdc.cncb.ac.cn/omix/preview/JxfeoEw1) and OMIX015926 (preview link: https://ngdc.cncb.ac.cn/omix/preview/HsnpF6Wj).

References

1 Sangiorgio, G., Calvo, M., Migliorisi, G., Campanile, F. & Stefani, S. The Impact of Enterococcus spp. in the Immunocompromised Host: A Comprehensive Review. *Pathogens* **13** (2024). https://doi.org/10.3390/pathogens13050409

2 Stringer, A. M. *et al.* Updated perspectives on the contribution of the microbiome to the pathogenesis of mucositis using the MASCC/ISOO framework. *Support Care Cancer* **32**, 558 (2024). https://doi.org/10.1007/s00520-024-08752-4

3 Martinelli, F. & Thiele, I. Microbial metabolism marvels: a comprehensive review of microbial drug transformation capabilities. *Gut Microbes* **16**, 2387400 (2024). https://doi.org/10.1080/19490976.2024.2387400

4 Alexander, J. L. *et al.* Gut microbiota modulation of chemotherapy efficacy and toxicity. *Nat Rev Gastroenterol Hepatol* **14**, 356–365 (2017). https://doi.org/10.1038/nrgastro.2017.20

5 Chrysostomou, D., Roberts, L. A., Marchesi, J. R. & Kinross, J. M. Gut Microbiota Modulation of Efficacy and Toxicity of Cancer Chemotherapy and Immunotherapy. *Gastroenterology* **164**, 198–213 (2023). https://doi.org/10.1053/j.gastro.2022.10.018

6 Yan, Y., Nguyen, L. H., Franzosa, E. A. & Huttenhower, C. Strain-level epidemiology of microbial communities and the human microbiome. *Genome Med* **12**, 71 (2020). https://doi.org/10.1186/s13073-020-00765-y

7 Kalan, L. R. *et al.* Strain- and Species-Level Variation in the Microbiome of Diabetic Wounds Is Associated with Clinical Outcomes and Therapeutic Efficacy. *Cell Host Microbe* **25**, 641–655.e645 (2019). https://doi.org/10.1016/j.chom.2019.03.006

8 Tričković, M., Kieser, S., Zdobnov, E. M. & Trajkovski, M. Subspecies of the human gut microbiota carry implicit information for in-depth microbiome research. *Cell Host Microbe* **33**, 1446–1458.e1444 (2025). https://doi.org/10.1016/j.chom.2025.07.015

9 Longley, D. B., Harkin, D. P. & Johnston, P. G. 5-fluorouracil: mechanisms of action and clinical strategies. *Nat Rev Cancer* **3**, 330–338 (2003). https://doi.org/10.1038/nrc1074

10 Spanogiannopoulos, P. *et al.* Host and gut bacteria share metabolic pathways for anti-cancer drug metabolism. *Nat Microbiol* **7**, 1605–1620 (2022). https://doi.org/10.1038/s41564-022-01226-5

11 Xu, W. *et al.* PreTA-mediated metabolism of 5-fluorouracil by intratumoral Citrobacter freundii drives chemoresistance in pancreatic cancer. *Cell Reports* **44** (2025). https://doi.org/10.1016/j.celrep.2025.116473

12 Almeida-Santos, A. C., Novais, C., Peixe, L. & Freitas, A. R. Enterococcus spp. as a Producer and Target of Bacteriocins: A Double-Edged Sword in the Antimicrobial Resistance Crisis Context. *Antibiotics (Basel)* **10** (2021). https://doi.org/10.3390/antibiotics10101215

13 Foladori, P. *et al.* SARS-CoV-2 from faeces to wastewater treatment: What do we know? A review. *Science of The Total Environment* **743** (2020). https://doi.org/10.1016/j.scitotenv.2020.140444

14 Spanogiannopoulos, P. *et al.* Host and gut bacteria share metabolic pathways for anti-cancer drug metabolism. *Nature Microbiology* **7**, 1605–1620 (2022). https://doi.org/10.1038/s41564-022-01226-5

15 Diógenes, E. M. *et al.* Effect of 5-fluorouracil on Escherichia coli and Enterococcus spp.: insights into the selective pressures caused by this cytotoxic drug. *Microbial Pathogenesis* **206** (2025). https://doi.org/10.1016/j.micpath.2025.107701

16 Zhang, M. *et al.* Anticancer agent 5-fluorouracil reverses meropenem resistance in carbapenem-resistant Gram-negative pathogens. *International Journal of Antimicrobial Agents* **64** (2024). https://doi.org/10.1016/j.ijantimicag.2024.107337

17 Fernandez-Marcos, P. J. & Nóbrega-Pereira, S. NADPH: new oxygen for the ROS theory of aging. *Oncotarget* **7**, 50814–50815 (2016). https://doi.org/10.18632/oncotarget.10744

18 Brown, S., Santa Maria, J. P. & Walker, S. Wall Teichoic Acids of Gram-Positive Bacteria. *Annual Review of Microbiology* **67**, 313–336 (2013). https://doi.org/10.1146/annurev-micro-092412-155620

19 Pereira, M. P. & Brown, E. D. Bifunctional catalysis by CDP-ribitol synthase: convergent recruitment of reductase and cytidylyltransferase activities in Haemophilus influenzae and Staphylococcus aureus. *Biochemistry* **43**, 11802–11812 (2004). https://doi.org/10.1021/bi048866v

20 Baur, S., Marles-Wright, J., Buckenmaier, S., Lewis, R. J. & Vollmer, W. Synthesis of CDP-activated ribitol for teichoic acid precursors in Streptococcus pneumoniae. *J Bacteriol* **191**, 1200–1210 (2009). https://doi.org/10.1128/jb.01120-08

21 Djorić, D., Little, J. L. & Kristich, C. J. Multiple Low-Reactivity Class B Penicillin-Binding Proteins Are Required for Cephalosporin Resistance in Enterococci. *Antimicrob Agents Chemother* **64** (2020). https://doi.org/10.1128/aac.02273-19

22 Arbeloa, A. *et al.* Role of class A penicillin-binding proteins in PBP5-mediated beta-lactam resistance in Enterococcus faecalis. *J Bacteriol* **186**, 1221–1228 (2004). https://doi.org/10.1128/jb.186.5.1221-1228.2004

23 Paulsen, I. T. *et al.* Role of mobile DNA in the evolution of vancomycin-resistant Enterococcus faecalis. *Science* **299**, 2071–2074 (2003).

24 Wei, L., Wen, X. S. & Xian, C. J. Chemotherapy-Induced Intestinal Microbiota Dysbiosis Impairs Mucosal Homeostasis by Modulating Toll-like Receptor Signaling Pathways. *Int J Mol Sci* **22** (2021). https://doi.org/10.3390/ijms22179474

25 van Vliet, M. J., Harmsen, H. J., de Bont, E. S. & Tissing, W. J. The role of intestinal microbiota in the development and severity of chemotherapy-induced mucositis. *PLoS Pathog* **6**, e1000879 (2010). https://doi.org/10.1371/journal.ppat.1000879

26 Dapa, T. *et al.* Within-host evolution of the gut microbiome. *Curr Opin Microbiol* **71**, 102258 (2023). https://doi.org/10.1016/j.mib.2022.102258

27 Forster, S. C. *et al.* A human gut bacterial genome and culture collection for improved metagenomic analyses. *Nat Biotechnol* **37**, 186–192 (2019). https://doi.org/10.1038/s41587-018-0009-7

28 Chen, D. W. & Garud, N. R. Rapid evolution and strain turnover in the infant gut microbiome. *Genome Res* **32**, 1124–1136 (2022). https://doi.org/10.1101/gr.276306.121

29 Trepka, K. R. *et al.* Expansion of a bacterial operon during cancer treatment ameliorates fluoropyrimidine toxicity. *Sci Transl Med* **17**, eadq8870 (2025). https://doi.org/10.1126/scitranslmed.adq8870

30 Zhang, M. *et al.* Deciphering the Antibacterial Mechanisms of 5-Fluorouracil in Escherichia coli through Biochemical and Transcriptomic Analyses. *Antibiotics (Basel)* **13** (2024). https://doi.org/10.3390/antibiotics13060528

31 Nathan, C. & Cunningham-Bussel, A. Beyond oxidative stress: an immunologist's guide to reactive oxygen species. *Nat Rev Immunol* **13**, 349–361 (2013). https://doi.org/10.1038/nri3423

32 Nguyen, G. T., Green, E. R. & Mecsas, J. Neutrophils to the ROScue: Mechanisms of NADPH Oxidase Activation and Bacterial Resistance. *Front Cell Infect Microbiol* **7**, 373 (2017). https://doi.org/10.3389/fcimb.2017.00373

33 Daca, A. & Jarzembowski, T. From the Friend to the Foe-Enterococcus faecalis Diverse Impact on the Human Immune System. *Int J Mol Sci* **25** (2024). https://doi.org/10.3390/ijms25042422

34 Spaans, S. K., Weusthuis, R. A., van der Oost, J. & Kengen, S. W. NADPH-generating systems in bacteria and archaea. *Front Microbiol* **6**, 742 (2015). https://doi.org/10.3389/fmicb.2015.00742

35 Seixas, A. F. *et al.* Bacterial Response to Oxidative Stress and RNA Oxidation. *Front Genet* **12**, 821535 (2021). https://doi.org/10.3389/fgene.2021.821535

36 Day, T., Huijben, S. & Read, A. F. Is selection relevant in the evolutionary emergence of drug resistance? *Trends Microbiol* **23**, 126–133 (2015). https://doi.org/10.1016/j.tim.2015.01.005

37 Ladjouzi, R., Lucau-Danila, A., Benachour, A. & Drider, D. A Leaderless Two-Peptide Bacteriocin, Enterocin DD14, Is Involved in Its Own Self-Immunity: Evidence and Insights. *Front Bioeng Biotechnol* **8**, 644 (2020). https://doi.org/10.3389/fbioe.2020.00644

38 Fiore, E., Van Tyne, D. & Gilmore, M. S. Pathogenicity of Enterococci. *Microbiol Spectr* **7** (2019). https://doi.org/10.1128/microbiolspec.GPP3-0053-2018

39 Anderson, B. D. & Bisanz, J. E. Challenges and opportunities of strain diversity in gut microbiome research. *Front Microbiol* **14**, 1117122 (2023). https://doi.org/10.3389/fmicb.2023.1117122

40 Hillege, L. E. *et al.* Microbial vitamin biosynthesis links gut microbiota dynamics to chemotherapy toxicity. *mBio* **16**, e0093025 (2025). https://doi.org/10.1128/mbio.00930-25

41 Xavier, J. B. Ecological management of the microbiota in patients with cancer. *Nat Rev Clin Oncol* **22**, 627–639 (2025). https://doi.org/10.1038/s41571-025-01049-3

42 Roggiani, S. *et al.* Gut microbiota resilience and recovery after anticancer chemotherapy. *Microbiome Res Rep* **2**, 16 (2023). https://doi.org/10.20517/mrr.2022.23

43 Hillege, L. E. *et al.* Metagenomic analysis during capecitabine therapy reveals microbial chemoprotective mechanisms and predicts drug toxicity in colorectal cancer patients. *medRxiv* (2024). https://doi.org/10.1101/2024.10.11.24315249

44 Vigneswaran, N. *et al.* Changing antimicrobial prescribing patterns, and laboratory reporting in Enterococcus faecalis infective endocarditis at a tertiary Australian centre. *Eur J Clin Microbiol Infect Dis* (2025). https://doi.org/10.1007/s10096-025-05331-1

45 Holleran, J. L., Eiseman, J. L., Parise, R. A., Kummar, S. & Beumer, J. H. LC-MS/MS assay for the quantitation of FdCyd and its metabolites FdUrd and FU in human plasma. *J Pharm Biomed Anal* **129**, 359–366 (2016). https://doi.org/10.1016/j.jpba.2016.07.027

46 Radovanovic, M., Schneider, J. J., Shafiei, M., Martin, J. H. & Galettis, P. Measurement of 5- fluorouracil, capecitabine and its metabolite concentrations in blood using volumetric absorptive microsampling technology and LC-MS/MS. *J Chromatogr B Analyt Technol Biomed Life Sci* **1188**, 123075 (2022). https://doi.org/10.1016/j.jchromb.2021.123075

47 Knijff, E., Dellaglio, F., Lombardi, A., Andrighetto, C. & Torriani, S. Rapid identification of Enterococcus durans and Enterococcus hirae by PCR with primers targeted to the ddl genes. *J Microbiol Methods* **47**, 35–40 (2001). https://doi.org/10.1016/s0167-7012(01)00297-4

48 Bulacio Mde, L., Galván, L. R., Gaudioso, C., Cangemi, R. & Erimbaue, M. I. Enterococcus Faecalis Biofilm. Formation and Development in Vitro Observed by Scanning Electron Microscopy. *Acta Odontol Latinoam* **28**, 210–214 (2015).

49 Abramson, J. *et al.* Accurate structure prediction of biomolecular interactions with AlphaFold 3. *Nature* **630**, 493–500 (2024). https://doi.org/10.1038/s41586-024-07487-w

50 van Kempen, M. *et al.* Fast and accurate protein structure search with Foldseek. *Nat Biotechnol* **42**, 243–246 (2024). https://doi.org/10.1038/s41587-023-01773-0

51 Wang, X. *et al.* Proteomic analysis of the Enterococcus faecalis V583 strain and clinical isolate V309 under vancomycin treatment. *J Proteome Res* **9**, 1772–1785 (2010). https://doi.org/10.1021/pr901216e

52 Cathro, P., McCarthy, P., Hoffmann, P., Kidd, S. & Zilm, P. Enterococcus faecalis V583 cell membrane protein expression to alkaline stress. *FEMS Microbiol Lett* **369** (2022). https://doi.org/10.1093/femsle/fnac082

53 Zhang, H., Zeng, X., Yin, Y. & Zhu, Z. J. Knowledge and data-driven two-layer networking for accurate metabolite annotation in untargeted metabolomics. *Nat Commun* **16**, 8118 (2025). https://doi.org/10.1038/s41467-025-63536-6

54 Jávega, B., Herrera, G. & O'Connor, J. E. Flow Cytometric Analysis of Oxidative Stress in Escherichia coli B Strains Deficient in Genes of the Antioxidant Defence. *Int J Mol Sci* **23** (2022). https://doi.org/10.3390/ijms23126537

55 Kho, K. & Meredith, T. C. Extraction and Analysis of Bacterial Teichoic Acids. *Bio Protoc* **8**, e3078 (2018). https://doi.org/10.21769/BioProtoc.3078

56 Hirt, H. *et al.* Enterococcus faecalis Sex Pheromone cCF10 Enhances Conjugative Plasmid Transfer In Vivo. *mBio* **9** (2018). https://doi.org/10.1128/mBio.00037-18

57 Ju, Y. *et al.* Inactivation of glutathione S-transferase alpha 4 blocks Enterococcus faecalis-induced bystander effect by promoting macrophage ferroptosis. *Gut Microbes* **17**, 2451090 (2025). https://doi.org/10.1080/19490976.2025.2451090

58 Amorim, N. *et al.* Refining a Protocol for Faecal Microbiota Engraftment in Animal Models After Successful Antibiotic-Induced Gut Decontamination. *Front Med (Lausanne)* **9**, 770017 (2022). https://doi.org/10.3389/fmed.2022.770017

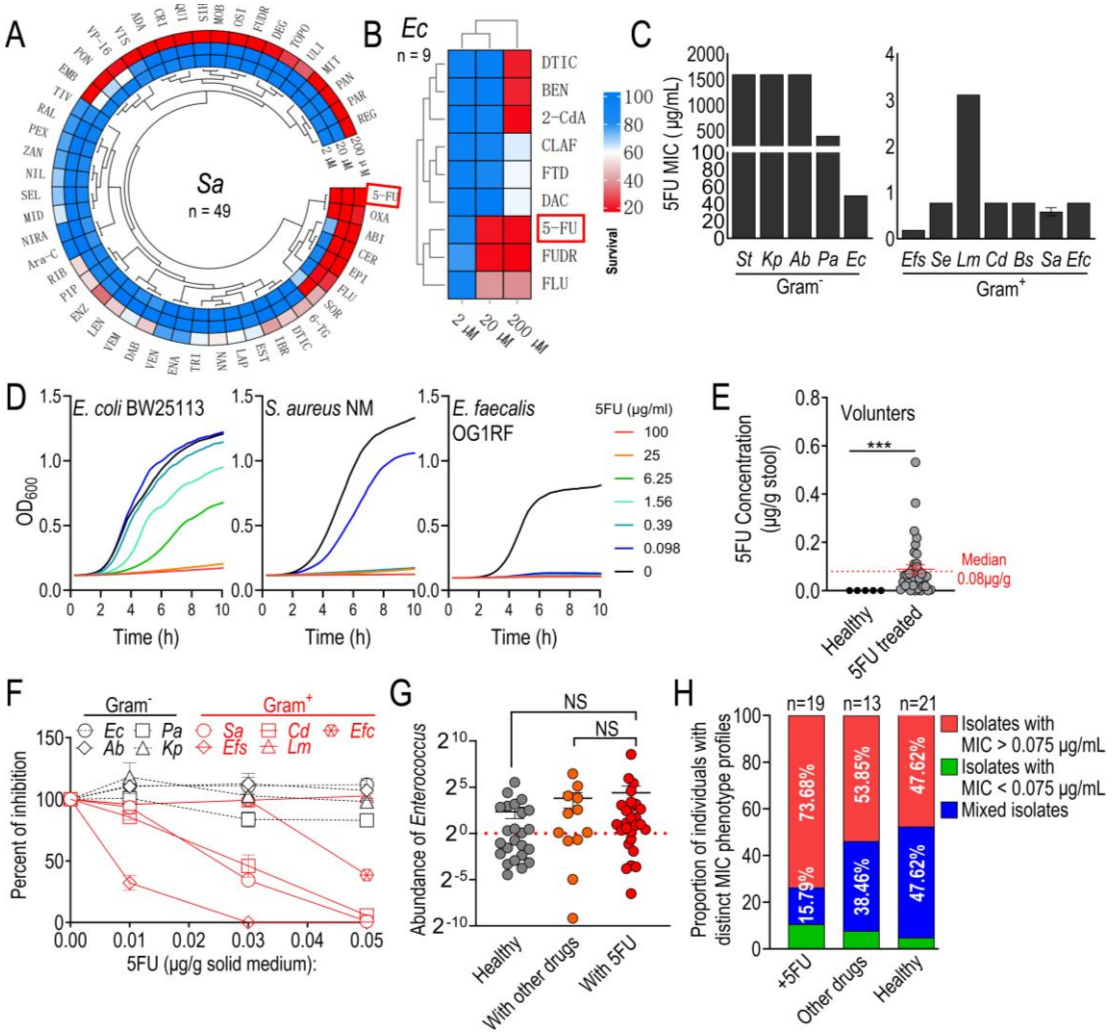

Fig. 1. Systematic screening and pharmacologically relevant exposure identify 5FU as a selective driver of strain-level remodeling in *E. faecalis* **(A and B)** Screening of an FDA-approved anticancer compound library identifies selective antibacterial activity. A total of 217 compounds were tested against the Gram-positive bacterium *S. aureus* Newman (*Sa*) **(A)** and the Gram-negative bacterium *E. coli* BW25113 (*Ec*) **(B)**. Heatmaps display growth inhibition (blue, low; red, high), with compounds shown that inhibited bacterial growth by at least 20%. **(C)** 5FU exhibits differential antibacterial activity across species. MICs were determined against a panel of clinically relevant Gram-negative (*S. typhimurium*, *St*; *K. pneumoniae*, *Kp*; *A. baumannii*, *Ab*; *P. aeruginosa*, Pa; *E. coli*, Ec) and Gram-positive bacteria (*E. faecalis*, *Efs*; *S. epidermidis*, *Se*; *L. monocytogenes*, *Lm*; *C. diphtheriae*, *Cd*; *B. subtilis*, *Bs*; *S. aureus*, *Sa*; *E. faecium*, *Efc*). Bars indicate MIC values (μg/mL). **(D)** Species-specific growth responses to 5FU. Representative growth curves of *E. coli*, *S. aureus*, and *E. faecalis* cultured in the presence of increasing concentrations of 5FU (0-100 μg/mL). **(E)** Detection of 5FU in human stool samples. 5FU concentrations (μg/g stool) were quantified by LC-MS/MS in samples from healthy individuals (n = 5) and cancer patients receiving 5FU treatment (n = 36). Each dot represents an individual; dashed horizontal lines indicate the median.

(F) Antibacterial effects at fecal-relevant concentrations. Survival of indicated Gram-positive and Gram-negative bacteria on TSA plates supplemented with 5FU at concentrations (0.01-0.08 μg/g) corresponding to the range detected in patient stool samples. **(G)** Enterococcus abundance in the human gut microbiota. Relative abundance of *Enterococcus* spp. was quantified by qRT-PCR in fecal samples from healthy individuals (n = 24), patients treated with 5FU (n = 27), and patients receiving other therapies (n = 12). Values were normalized to total bacterial load. **(H)** Distribution of 5FU susceptibility among intestinal *E. faecalis* isolates. Individuals were classified based on the presence of low-MIC strains (MIC < 0.075 μg/mL, green), high-MIC strains (MIC > 0.075 μg/mL, red), or mixed populations (blue) across healthy (n = 21), other treatment (n = 13), and 5FU-treated groups (n = 19). Data are presented as mean ± SEM. Significant difference (***p < 0.001) was identified in E by two-tailed Mann-Whitney U test.

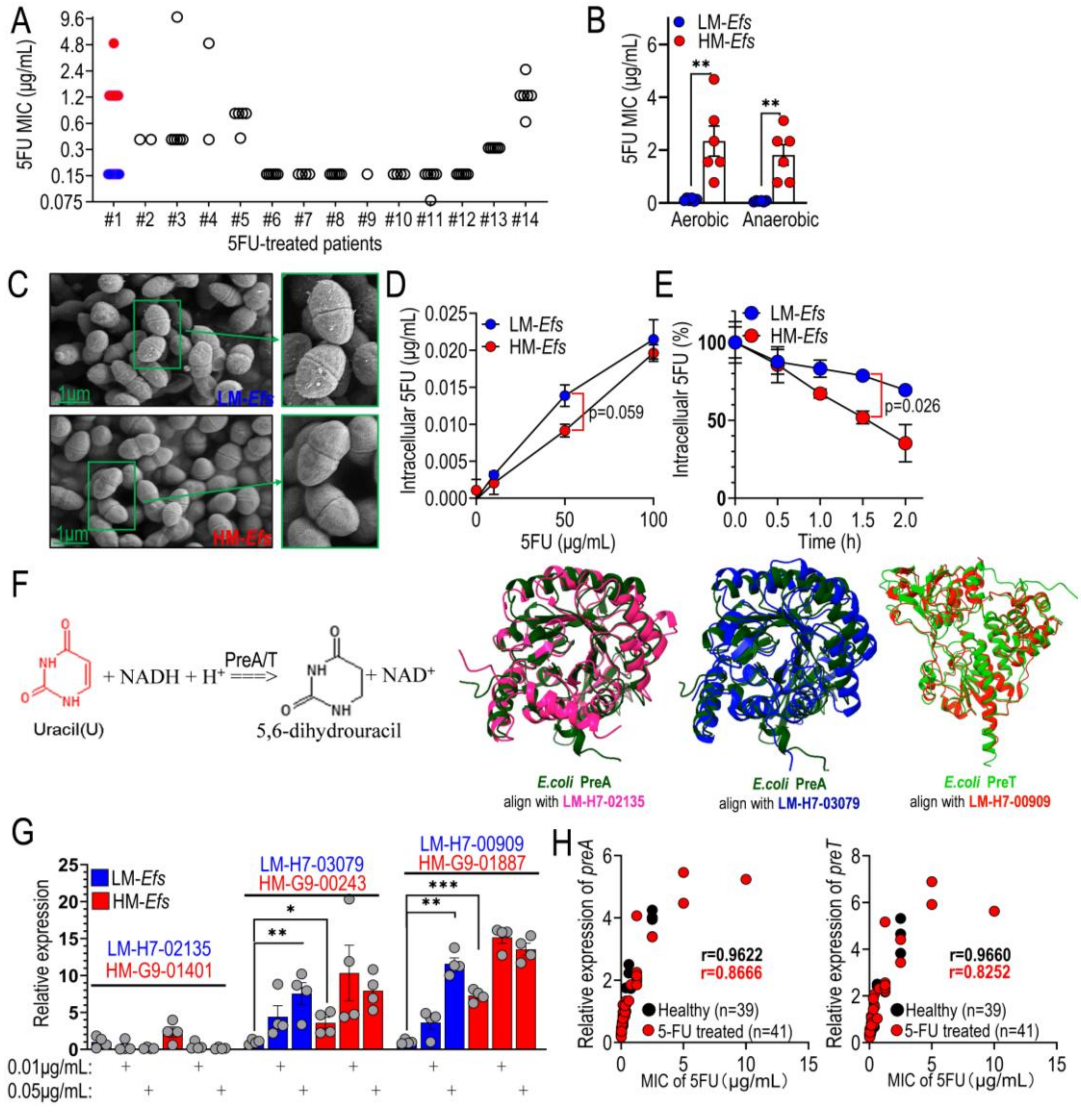

Fig. 2. PreTA-like enzymatic detoxification mediates 5FU resistance in *E. faecalis*. (A) Distribution of 5FU MICs among *E. faecalis* clinical isolates from patients receiving 5FU treatment (n = 14). All selected patients harbored isolates with MIC values above the threshold of 0.075 μg/mL. One representative patient (#1) exhibited two distinct subpopulations, comprising low-MIC (LM-*Efs*, blue) and high-MIC (HM-*Efs*, red) strains. **(B)** Comparison of 5FU susceptibility under aerobic and anaerobic conditions. MIC values were determined for LM-*Efs* and HM-*Efs* strains, showing consistent resistance differences across oxygen conditions. **(C)** Scanning electron microscopy (SEM) of LM-*Efs* and HM-*Efs* strains reveals altered cell surface morphology. Scale bar, 1 μm. **(D)** Intracellular accumulation of 5FU in LM-*Efs* and HM-*Efs* following exposure to increasing concentrations of 5FU. **(E)** Time-dependent retention of intracellular 5FU following pulse exposure. Cells were incubated with 5FU and subsequently washed, and intracellular 5FU levels were quantified over time in LM-*Efs* and HM-*Efs* strains. **(F)** Structural prediction of enzymes involved in 5FU metabolism identifies PreTA-like homologs in LM-*Efs* and HM-*Efs* genomes. **(G)** Relative expression of PreTA-like genes in LM-*Efs* and HM-*Efs*

in the presence or absence of 5FU. **(H)** Correlation between PreTA-like gene expression and 5FU MIC across *E. faecalis* isolates from healthy individuals (black) and 5FU-treated patients (red), showing a strong positive association. Data are presented as mean ± SEM. Significant differences (*p < 0.05, **p < 0.01, and ***p < 0.001) were identified in B, D, and E by two-tailed Student's *t* test and in G by one-way ANOVA analysis.

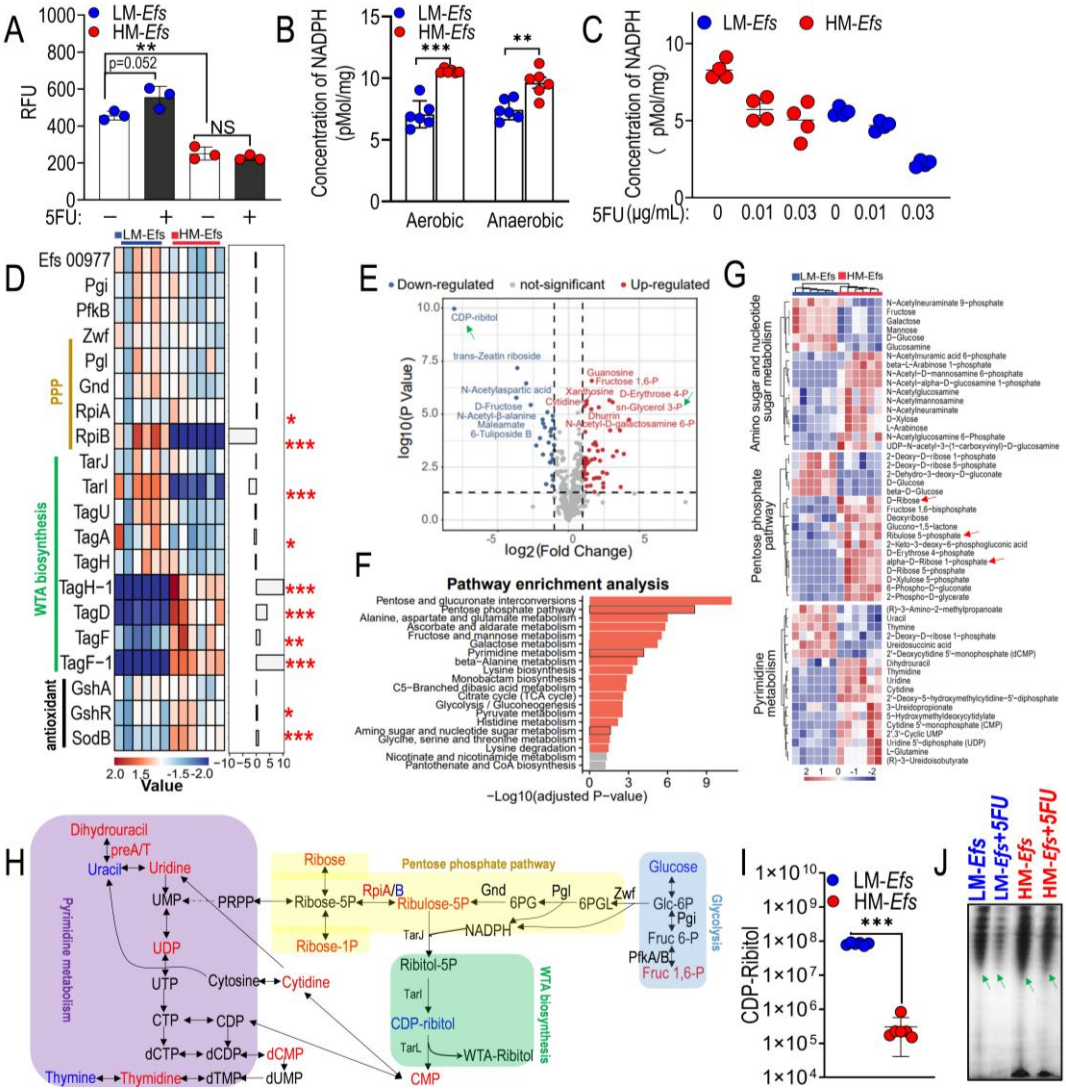

Fig. 3. Reprogramming of NADPH metabolism and redox homeostasis underlies stress tolerance in 5FU-resistant *E. faecalis*. (A) Intracellular reactive oxygen species (ROS) levels, measured as relative fluorescence units (RFU), in LM-*Efs* and HM-*Efs* with or without 5FU treatment. **(B)** Intracellular NADPH concentrations (pmol/mg protein) in LM-*Efs* and HM-*Efs* under aerobic and anaerobic conditions. **(C)** Dose-dependent changes in NADPH levels in LM-*Efs* and HM-*Efs* following exposure to increasing concentrations of 5FU. **(D)** Proteomic profiling reveals differential abundance of proteins involved in wall teichoic acid (WTA) biosynthesis and antioxidant pathways in LM-*Efs* and HM-*Efs*. **(E)** Volcano plot of differentially abundant metabolites between LM-*Efs* and HM-*Efs* (red, upregulated; blue, downregulated; grey, not significant). **(F)** Pathway enrichment analysis of significantly altered metabolites highlights metabolic and biosynthetic pathways associated with WTA biosynthesis and redox balance. **(G)** Heatmap showing changes in metabolites associated with amino sugar, nucleotide sugar, and pentose phosphate pathways. **(H)** Schematic overview of integrated metabolic pathways linking pyrimidine metabolism, the pentose phosphate pathway, and WTA biosynthesis. **(I)**

Abundance of the WTA precursor CDP-ribitol in LM-*Efs* and HM-*Efs*. **(J)** WTA abundance in LM-*Efs* and HM-*Efs* with or without 5FU treatment. Data are presented as mean ± SEM. Significant differences (*p < 0.05, **p < 0.01, and ***p < 0.001) were identified in A by one-way ANOVA analysis and in B, D, and I by two-tailed Student's *t* test.

A

Abbreviation	Full Name	Class	ARGs in LM-*Efs*	ARGs in HM-*Efs*
TIG	Tigecycline	Glycylcycline (Tetracycline derivative)	*tet(M)_10*	*tet(M)_10,tet(L)_2*
ERM	Erythromycin	Macrolide	*erm(B)_18*	*erm(B)_18*
KAN	Kanamycin	Aminoglycoside	*aph(3')-III_1,aac(6')-aph(2'')_1*	*aph(3')-III_1*
LINC	Lincomycin	Lincosamides	*lsa(A)_1*	*lsa(A)_3*
TMP	Trimethoprim	dihydrofolate reductase inhibitor	N/A	*dfrG_1*
LIN	Linezolid	Oxazolidinone	N/A	*optrA_15*
LEV	Levofloxacin	Fluoroquinolone	N/A	N/A
CFX	Cefuroxime	Cephalosporin (Beta-lactam)	N/A	N/A
CTX	Cefotaxime	Cephalosporin (Beta-lactam)	N/A	N/A
CHL	Chloramphenicol	Phenicol	N/A	*cat_5,fexA_1*
TET	Tetracycline	Tetracycline	*tet(M)_10*	*tet(M)_10,tet(L)_2*

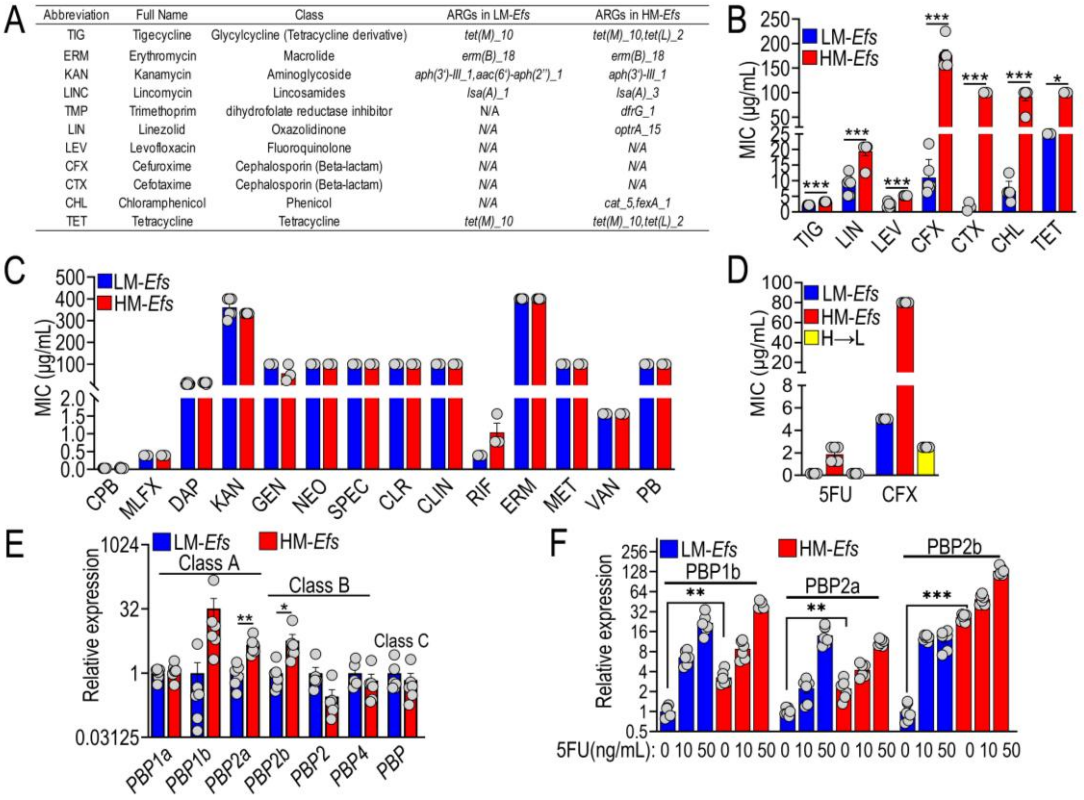

Fig. 4. 5FU-selected *E. faecalis* exhibit increased tolerance to clinically relevant antibiotics. (A) Summary of antibiotic resistance profiles. Table listing antibiotic names, classes, and corresponding resistance genes identified in LM-*Efs* and HM-*Efs* isolates. **(B and C)** Increased antibiotic tolerance in HM-Efs. MICs (μg/mL) of indicated antibiotics were determined for LM-Efs and HM-Efs strains. **(D)** Lack of transferable resistance by plasmid conjugation. MICs of 5FU and CFX were measured in LM-*Efs* strains following acquisition of plasmids from HM-*Efs*, showing no significant transfer of resistance. **(E)** Differential expression of penicillin-binding protein (PBP) genes. Relative expression levels (fold change) of genes encoding distinct PBP classes were quantified in LM-*Efs* and HM-*Efs*. **(F)** Induction of PBP gene expression by 5FU. Relative expression of PBP-encoding genes in LM-*Efs* and HM-*Efs* following exposure to increasing concentrations of 5FU. Data are presented as mean ± SEM. Significant differences (*$p < 0.05$, **$p < 0.01$, and ***$p < 0.001$) were identified in B and E by two-tailed Student's *t* test and in F by one-way ANOVA analysis.

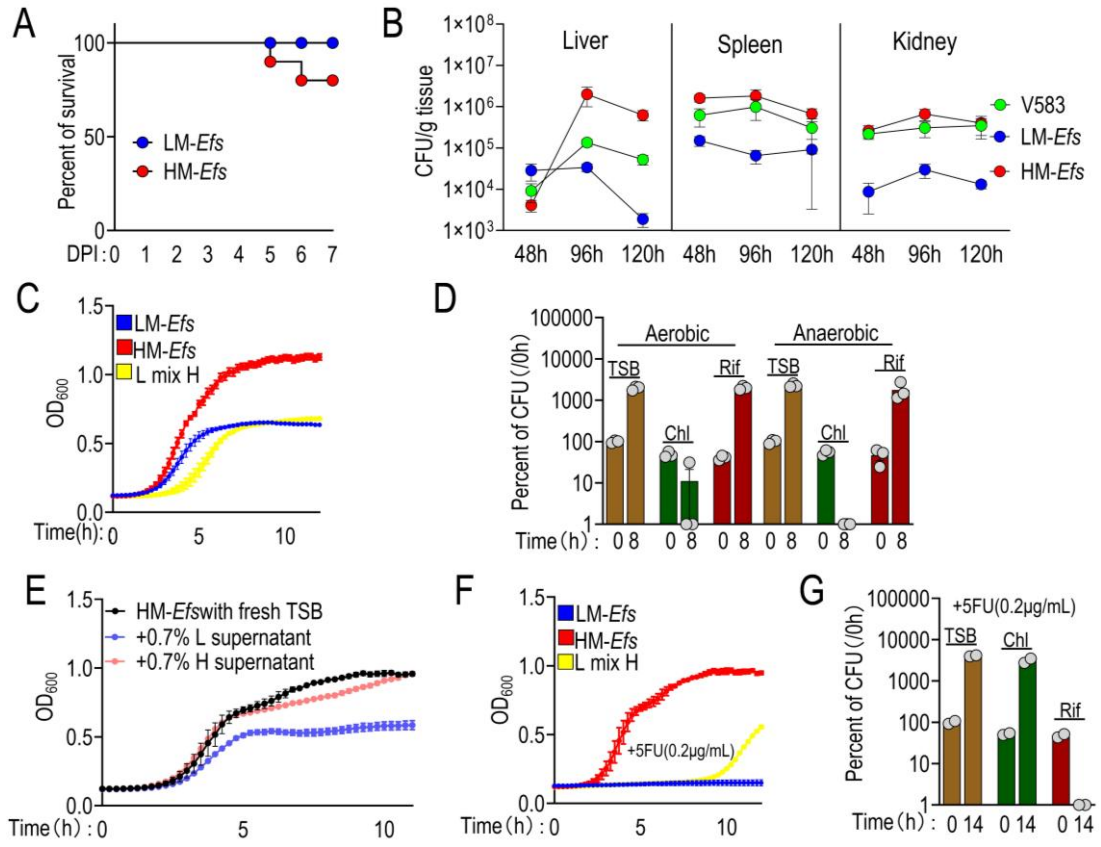

Fig. 5. Competitive interactions shape strain dominance and virulence potential in *E. faecalis*. (A) Survival of mice following intravenous infection with LM-*Efs* or HM-*Efs*. Kaplan-Meier survival curves over 7 days post-infection (DPI). **(B)** Bacterial burden in infected tissues. CFU (per g tissue) in the liver, spleen, and kidney at the indicated time points following infection with 4×10^8 CFU of V583 (reference strain), LM-*Efs*, or HM-*Efs*. **(C)** Growth dynamics of LM-*Efs* and HM-*Efs* in monoculture and co-culture. Growth curves of LM-*Efs*, HM-*Efs*, and a 1:1 mixed culture in TSB. **(D)** Competitive fitness under different oxygen conditions. Relative CFUs of LM-*Efs* and HM-*Efs* in co-culture were quantified under aerobic and anaerobic conditions. **(E)** Conditioned medium-dependent modulation of growth. Growth of HM-*Efs* in fresh TSB (control) or TSB supplemented with 0.7% supernatant derived from LM-*Efs* or HM-*Efs* cultures. **(F)** 5FU-dependent competitive dynamics. Growth curves of LM-*Efs*, HM-*Efs*, and mixed cultures in the presence or absence of 5FU (0.2 μg/mL). **(G)** 5FU-driven shifts in population composition. Relative proportions of LM-*Efs* and HM-*Efs* over time in co-culture following 5FU treatment (0.2 μg/mL), expressed as percentage of total CFU. Data are presented as mean ± SEM.

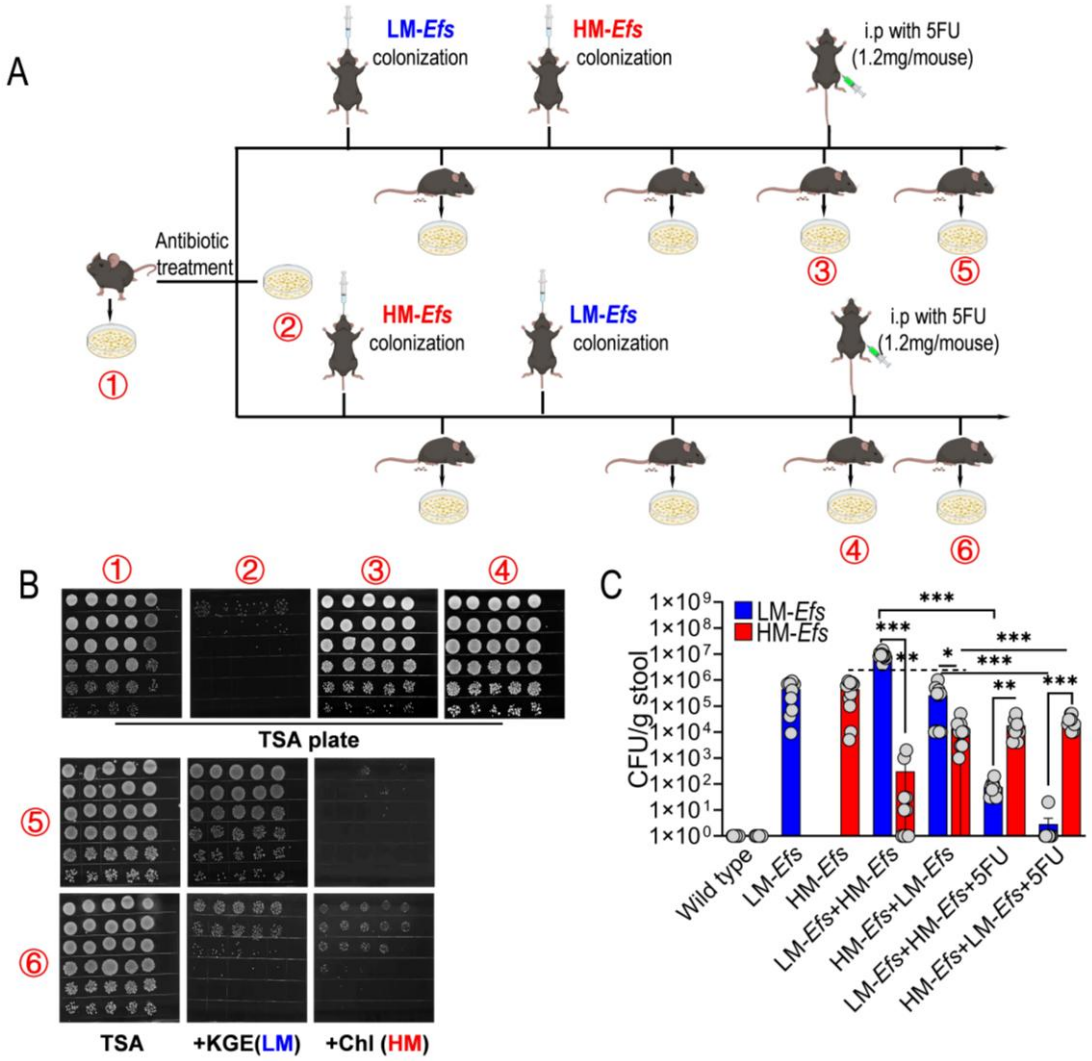

Fig. 6. 5FU treatment drives *in vivo* competitive expansion of resistant and virulent *E. faecalis* lineages. (A) Schematic of the *in vivo* competition model. Antibiotic-pretreated mice were first orally gavaged with LM-*Efs* or HM-*Efs*, followed by a second gavage with the reciprocal strain to establish sequential colonization. Mice were then treated with intraperitoneal 5FU or vehicle control. Fecal samples were collected longitudinally for analysis. **(B)** Representative TSA plates showing colony-forming units (CFUs) recovered from fecal samples at indicated time points and treatment conditions. **(C)** Quantification of *in vivo* competitive colonization. CFUs per g feces of LM-*Efs* and HM-*Efs* were determined over time (n = 5 mice per group), demonstrating preferential expansion of HM-*Efs* following 5FU treatment. Data are presented as mean ± SEM. Significant differences (*p < 0.05, **p < 0.01, and ***p < 0.001) were identified in C by two-way ANOVA analysis.